ISSN 0040-5795, Theoretical Foundations of Chemical Engineering, 2016, Vol. 50, No. 4, pp. 498–507. © Pleiades Publishing, Ltd., 2016.
Original Russian Text © T.A. Sedneva, M.L. Belikov, E.P. Lokshin, A.T. Belyaevskii, 2015, published in Khimicheskaya Tekhnologiya, 2015, Vol. 16, No. 7, pp. 398–407.

Synthesis and Study of Photocatalytic Oxide Nanocomposites of Titanium(IV) and Cobalt(II)

T. A. Sedneva*, M. L. Belikov, E. P. Lokshin, and A. T. Belyaevskii

Tananaev Institute of Chemistry and Technology of Rare Elements and Mineral Resources, Kola Scientific Center, Russian Academy of Sciences, Apatity, Russia

**e-mail: sedneva@chemy.kolasc.net.ru*

Received August 1, 2014

Abstract—The phase formation, texture, and photocatalytic activity of synthesized oxide nanocomposites of titanium(IV) and cobalt(II) have been studied in relation to the cobalt content and temperature of heat treatment. The high photocatalytic activity of optimum compositions has been recorded within the spectral range of visible light with $\lambda \geq 670$ nm.

Keywords: titanium dioxide, cobalt, modification, hydrolysis, nanocomposites, phase formation, texture, morphology, photocatalytic activity, spectral range

DOI: 10.1134/S0040579516040278

INTRODUCTION

Titanium dioxide is studied intensely, in particular due to its potential application in photocatalysis. However, pure TiO_2 has photocatalytic activity (PCA) mainly in the UV spectrum because of the considerable value of its forbidden bandwidth FBW = 3.1 eV. The expansion of the absorption spectrum of TiO_2 to the visible region ($\lambda \geq 400$–700 nm) would make it possible to use solar radiation more effectively. In connection with this, the development of methods for modifying the optical properties of TiO_2 is of great practical interest [1, 2].

Our previous works deal with the expansion of the spectral range of the PCA to the visible and infrared region by TiO_2 doped with inovalent W^{6+} and Nb^{5+} cations [3, 4]. However, we would like to offer the more available cobalt, the oxide FBW of which is 0.7 eV [5], which corresponds to the energy of waves that have lengths of 1770 nm.

There are relatively few descriptions of the synthesis and properties of photocatalytic dispersions of CoO/TiO_2. For example, the enhanced FCA of the CoO/TiO_2 nanotube composite, which was obtained by the cathode deposition in 0.05 M of $Co(NO_3)_2$ at TiO_2 carbon nanotubes (CNTs) calcined at 450°C is recorded in [6]. The increase in the FCA of C-doped TiO_2 powders obtained by the sol-gel method is also stated in [7]. Works [8, 9] present the ways of producing the photocatalytic films of TiO_2/C with improved characteristics due to the formation of a compact crystalline TiO_2 film, which also contains Co due to diffusion during high-temperature heat treatment (500–700°C). The known methods for synthesizing these structures by mechanical doping or chemical deposition of one compound at the powders of another, as well as the sol-gel method are not quite available due to various reasons, are complicated and often restrict the content of doping metal to 1–5%.

In this work, we assumed that the combined alkaline hydrolysis of Ti and Co salts may turn out to be easier and more efficient, also yielding the production of little-studied dispersions with a high cobalt content of 0.5–60 wt %.

The purpose of this work is to study the features of forming composites in the Ti–O–Co system for developing available photocatalysts (FCs) that are active in a visible spectral band.

EXPERIMENTAL

Composite materials were obtained during the combined hydrolysis of $TiCl_4$ and $CoCl_2$ salts in the ammonia water at a temperature of 20 ± 2°C similar to the procedures developed [3, 4]. When the concentration of the Co doping metal varied in the range of 0.5–60 wt % under the conditions of heat treatment by exposure to the air (80–1150°C), we obtained polyphase nanocomposites characterized by the methods of chemical analysis, XRF (DRON-3, CuK_α emission), BET by nitrogen (FlowSorb II 2300; TriStar 3020 *V*1.03), thermogravimetry in the atmosphere of argon at the rate of heating equal to 10°C/min in the Stepanov vessel with the isolated Pt–PtRh thermal couple (NETZSCH STA 409 PC/PG) and SEM (SEM LEO-420). The FCA of the samples was esti-

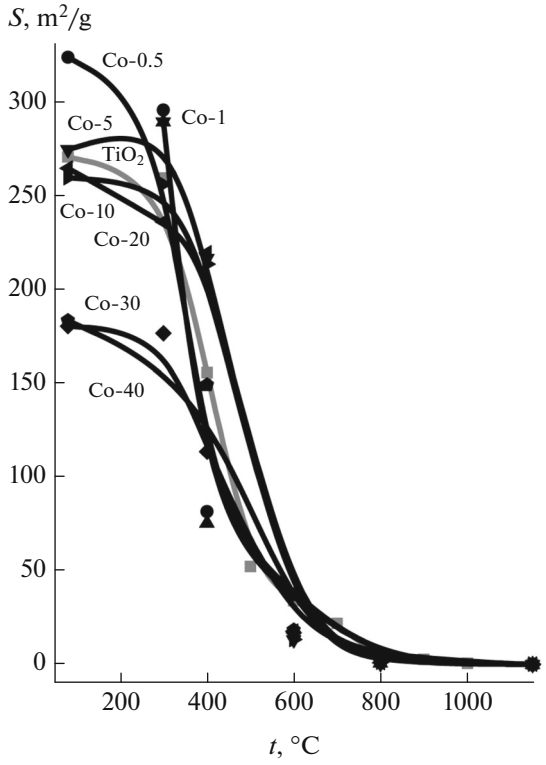

Fig. 1. Dependence of the surface area (S, m^2/g) of Co-modified titanium dioxide samples on heat treatment (t, °C) and doping.

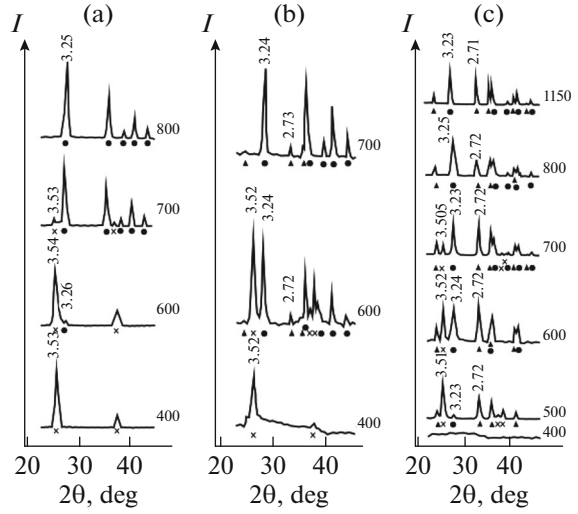

Fig. 2. Diffractograms for Co-modified titanium dioxide with respect to treatment temperature (numbers at the curves, °C) and to Co content: (a) 1; (b) 40 wt %. Phases: × is anatase, ● is rutile, ▲ is $CoTiO_3$.

mated photocolorimetrically (FEK-56 PM) by a degree of ferroin decoloration (the losses of indicator E content, %) at the visible and filtered flow of light. The marking of the sample, e.g., 400-Co-0.5 contains the data on the temperature of heat treatment, 400°C, the Co doping metal, and its degree of doping, 0.5 wt.

RESULTS AND DISCUSSION

Tables 1–3 and Figs. 1–9 present the summary of the experimental data on the change in the chemical and phase composition (XRF), the surface area (S, m^2/g), the average particle size (d, nm), the volume (V, cm^3/g), the depth (h, nm), and the diameter (D, nm) of the pores in relation to the conditions of heat treatment (t, °C) and the degree of doping in the C-modified samples of titanium dioxide, as well as the degree of FCA (E, %) in the reaction of degradation when the indicators are exposed to the full and filtered ($\lambda \geq 670$ nm) light.

The Co doping of TiO_2 in the amount of 0.5–60 wt % yields nanodisperse powders (7–12 nm) with a surface area of 180–320 m^2/g that contain up to 6.6 wt % of NH_4^+ and 1.06 wt % of Cl^-. At a low level of Co doping, which varies in the range of 0.5–1.0 wt %, the hydrolysis products contain approximately 79.9 wt % of TiO_2, which is close to the formula of titanium oxyhydroxide $TiO(OH)_2$ (81.6 wt % TiO_2). The increase in the temperature of heat treatment of hydrolysis products leads to the regular shrinkage of the surface area of the powders (Table 1, Fig. 1).

Phase Formation

According to the XRF data (Table 1, Fig. 2), hydrolysis forms X-ray amorphous products. Their heat treatment at 400–1150°C leads to several phase transitions that depend on the degree of Co doping. When Co doping is up to 1 wt %, XRF records only the formation of anatase (3.52 Å), then rutile (3.24 Å). As soon the Co doping exceeds 5 wt %, Co is separated as cobalt metatinatate $CoTiO_3$ (2.72 Å) at temperatures of the anatase-rutile phase transition.

The thermograms of the modified products (Fig. 3) are identical to the thermogram of TiO_2 that have similar genesis [10], which indicates the hydroxide origin of products that resulted from the combined hydrolysis of $TiCl_4$ and $CoCl_2$. All thermograms have similar DSC curves with only one endothermic effect, which indicates the dehydration of hydrolysis products, regardless of their degree of Co doping, which usually ends at a temperature of approximately 400°C and approximately 23–27% weight loss in the sample. The results of the chemical analysis indicate the simultaneous removal of volatile components as well, such as chloride ions and the ammonium group (Table 1).

For all hydrolysis products, each thermogram also has one expressed exothermal effect, which may indicate the simultaneous occurrence of crystallization

Table 1. Phase composition and physicochemical properties of composites in the Ti–O–Co system

Samples	t, °C	C, wt %				XRF	S, m^2/g	d, nm
		TiO_2	Cl^-	NH_4^+	Co^{2+}		BET	
80-Co-0.5	80	79.1	–	–	0.26	am	323	7.1
300-Co-0.5	300	–	n/d	0.45	–	am	295	7.8
400-Co-0.5	400	–	–	–	–	a	82	19
700-Co-0.5	700	–	–	–	–	20% a, 80% r	–	–
800-Co-0.5	800	–	–	–	–	r	1.05	1360
1150-Co-0.5	1150	–	–	–	–	r	0.24	5950
80-Co-1	80	78.6	–	–	0.43	am	–	–
300-Co-1	300	–	–	–	–	am	288	8.0
400-Co-1	400	–	–	–	–	a	75	20
500-Co-1	500	–	–	–	–	a	21	75
600-Co-1	600	98.8			0.97	99% a, 1% r	36	39
700-Co-1	700	–	–	–	–	10% a, 90% r	–	–
1150-Co-1	1150	–	–	–	–	r	0.21	6800
80-Co-5	80	79.8	–	3.28	1.67	am	274	8.4
400-Co-5	400	–	–	0.34	–	a, am	216	7.1
500-Co-5	500	–	–	–	–	95% a, 5% r	14	114
600-Co-5	600	94.7	–	–	4.9	a, r, $CoTiO_3$	13.4	111
800-Co-5	800	–	–	–	–	r,$CoTiO_3$	0.74	1930
1150-Co-5	1150	–	–	–	–	r, $CoTiO_3$	0.24	5950
80-Co-10	80	71.9	n/d	4.51	5.14	am	264	8.7
400-Co-10	400	–	–	0.46	–	am	219	10
500-Co-10	500	–	–	–	–	a, r, $CoTiO_3$	15	36
600-Co-10	600	88.8	n/d	n/d	9.84	a, r, $CoTiO_3$	18	55
700-Co-10	700	–	–	–	–	r,$CoTiO_3$	–	–
800-Co-10	800	–	–	–	–	r, $CoTiO_3$	1.17	1160
1150-Co-10	1150	–	–	–	–	r, $CoTiO_3$	0.35	2720
80-Co-20	80	–	–	–	–	am	259	8.9
400-Co-20	400	–	–	–	–	am	213	11
600-Co-20	600	80.2	–	–	19.8	a, r, $CoTiO_3$	13	74
700-Co-20	700	74.6	–	–	20.0	a, r, $CoTiO_3$	–	–
800-Co-20	800	–	–	–	–	r, $CoTiO_3$	1.33	747
1150-Co-20	1150	–	–	–	–	r, $CoTiO_3$	0.34	2820
80-Co-30	80	64.7	–	–	–	am	180	13
400-Co-30	400	–	0.3	0.15	–	am	113	20
600-Co-30	600	83.9	n/d	n/d		a, r, $CoTiO_3$	17	58
800-Co-30	800	–	–	–	–	r, $CoTiO_3$	4.54	211
1150-Co-30	1150					r, $CoTiO_3$	0.17	5640
80-Co-40	80	64.6	–	6.60	–	am	183	13
400-Co-40	400	–	–	0.20	–	am	149	16
500-Co-40	500	–	–	–	–	a, r, $CoTiO_3$	35	28
600-Co-40	600	76.8	–	–	–	a, r, $CoTiO_3$	19	53
800-Co-40	800	–	–	–	–	r, $CoTiO_3$	4.21	228
1150-Co-40	1150	–	–	–	–	r, $CoTiO_3$	0.12	9600
80-Co-60	80	–	–	–	–	–	254	9.1
400-Co-60	400	–	–	–	–	am	156	15
600-Co-60	600	41.9	–	–	45.7	a, r, $CoTiO_3$	21	73
800-Co-60	800	–	–	–	–	r, $CoTiO_3$	4.45	321
1110-Co-60	1150	–	–	–	–	r, $CoTiO_3$	0.11	9850

* am is amorphous, a is anatase, r is rutile, n/d is not detected, and "–" is not determined.

processes, such as the formation of cobalt-containing anatase and its transformation to rutile, followed by the separation of cobalt with part of titanium as metatitanate. The temperature of the exothermal crystallization maximum shifts from 412.2 to 527.3°C as the cobalt content increases from 0 to 40 wt %, which may be related to the individual features of Co, the oxide crystallization of which requires much energy expenditures. For example, when Co doping is 1 wt %, anatase crystallizes at just 400°C, whereas when the Co content is 5 wt %, its crystallization only begins to manifest against the background of the amorphous matrix. However, according to the XRF data, the metastable state of titanium dioxide in these samples is changed to rutile, followed by the formation of Co-containing crystalline phase $CoTiO_3$ already at 500°C. This phase transition is not marked by a exothermal effect. In the more doped products, the influence of cobalt is characterized by the continuing decrease in the temperature of the anatas-to-rutile crystal physical transformation and the separation of $CoTiO_3$. We may speak about the contributing influence of cobalt on the rutile formation process. We should mention that cobalt does not form independent crystalline phases of own oxides within the entire doping range, i.e., it is crystallized only as $CoTiO_3$.

Thus, the synthesis products in the Ti–O–Co system are characterized by the formation of approximately five polyphase zones, which depends on the doping and heat treatment (Fig. 4).

Table 2. Dependence of texture characteristics V (cm^3/g), h (nm), d (nm) for the Co-modified TiO_2 samples on cobalt content and heat treatment t, °C

t	V	h	D	t	V	h	D
Co-0,5				Co-1			
80	–	–	–	80	0.29	3.71	3.97
300	0.27	3.39	4.09	300	0.29	4.09	3.84
400	0.19	9.03	6.95	400	0.18	8.85	6.86
600	–	–	–	500	0.054	9.15	7.05
Co-5				Co-10			
80	0.26	3.93	4.12	80	0.22	3.60	4.11
300	0.29	4.11	3.99	300	0.22	3.79	3.96
400	0.28	4.96	4.32	400	0.26	4.60	4.20
500	0.042	10.4	8.82	500	0.049	11.4	9.76
Co-20				Co-30			
80	0.22	3.66	4.40	80	0.16	3.95	4.43
300	0.23	3.80	4.11	300	0.17	3.99	4.26
400	0.25	4.47	4.30	400	0.19	6.24	5.06
500	0.16	10.5	8.68	500	0.16	16.9	13.6
Co-40				Co-60			
80	0.15	3.75	4.18	80	0.158	2.98	3.40
400	0.19	4.94	4.33	300	–	–	–
500	0.16	17.5	13.8	400	0.173	4.49	3.78
600	–	–	–	600	0.158	28.41	24.75
800	0.019	7.9	20.4	800	0.024	8.30	20.96

Texture

The surface area of the Co-modified products with the Co doping enhancement up to 5 wt % exceeds the surface area of TiO_2, but then it decreases (Fig. 1), especially when the doping is above 30 wt %. This noticeable difference levels out after the dehydration ends and when the oxide systems begin to form, i.e., in the temperature range starting from 400–600°C. The values for the surface area scatter significantly in the X-ray-amorphous structures, varying from 180 to 330 m^2/g (13–7 nm), but their scattering goes down to 36–70 m^2/g (40–57 nm) in the mixed phases of cobalt anatase-rutile-metatitanate and to 0.1–4.5 m^2/g (0.3–10 μm) in the two-phase rutile–metatitanate composites with respect to the temperature. Thus, the both X-ray amorphous powders and polyphase composites have a developed surface and a nanosized character until they are treated at 800–900°C (Table 1). The powders that are calcined at higher temperatures are subject to agglomeration and have a micron character.

The texture characteristics of some of the synthesized composites that are presented in Table 2 and Fig. 5 point to their mesoporous character. The sorption isotherms of the both X-ray amorphous and crystalline samples have absorption-desorption S-shaped curves with hysteresis loops, which indicates their mesoporous character according to the IUPAC classification [11]. Samples with unfinished dehydration, e.g., 80–Co–5 and 300-Co–5, etc., have similar texture data. As the crystallization processes begin, the mesoporosity of the powders decreases. The sorption curves of the composites that are calcined at temperatures over 900°C hardly have hysteresis.

As the temperature of powder heat treatment increases, as a rule, the diameter D and the pore height h increase, whereas the surface area and the micropore volume V reduce (Table 2). The temperature dependence of a change in the micropore volume V at the temperatures of 100–300°C is similar to the change in the surface area, which is probably the result of the intense removal of water from the oxyhydroxide hydrolysis products. Here, the micropore volume of the X-ray amorphous products is 0.15–0.29 cm^3/g. As the temperature and the degree of doping continue to increase, V drops sharply, which is related to the processes of crystallization, aggregation, and finally agglomeration at temperatures over 800°C. For example, the micropore volume in the 800-Co-60 sample is only 0.024 cm^3/g. At the same time, we note that the increase in Co doping also maintains micropore sizes at increased temperatures.

Table 3. Dependence of PCA (E, %) for the TiO_2 Co-modified samples with respect to ferroin during exposure to visible and filtered light ($\lambda \geq 670$ nm) on the Co content, heat treatment, phase composition, and dispersion ability

Sample	RFA	d, nm	E, %,	
			visible light	$\lambda \geqslant 670$ nm
400-Cl	Anatase	9.9	94	47
80-Co-1	X-ray amorphous	–	96	78
400-Co-1	Anatase	20	82	61
600-Co-1	99% anatase, 1% rutile	39	77	59
800-Co-1	Rutile	1320	60	47
1150-Co-1	Rutile	6800	58	46
80-Co-5	X-ray amorphous	8.4	96	91
400-Co-5	X-ray amorphous, anatase	7.1	89	82
600-Co-5	Anatase, rutile, $CoTiO_3$	13	76	70
800-Co-5	Rutile, $CoTiO_3$	0.74	56	52
1150-Co-5	Rutile, $CoTiO_3$	0.24	54	49
80-Co-10	X-ray amorphous	8.7	100	96
400-Co-10	X-ray amorphous	10	92	89
600-Co-10	Anatase, rutile, $CoTiO_3$	55	81	77
800-Co-10	Rutile, $CoTiO_3$	1160	68	65
1150-Co-10	Rutile, $CoTiO_3$	2720	62	58
80-Co-20	X-ray amorphous	8.9	95	90
400-Co-20	X-ray amorphous	11	87	84
600-Co-20	Anatase, rutile, $CoTiO_3$	74	82	77
800-Co-20	Rutile, $CoTiO_3$	747	69	65
1150-Co-20	Rutile, $CoTiO_3$	2820	62	54
80-Co-40	X-ray amorphous	13	77	67
400-Co-40	X-ray amorphous	20	74	66
600-Co-40	Anatase, rutile, $CoTiO_3$	58	77	67
800-Co-40	Rutile, $CoTiO_3$	211	76	65
1150-Co-40	Rutile, $CoTiO_3$	5640	62	56
80-Co-60	X-ray amorphous	9.1	69	57
400-Co-60	X-ray amorphous	15	66	54
600-Co-60	Anatase, rutile, $CoTiO_3$	73	58	51
800-Co-60	Rutile, $CoTiO_3$	321	54	47
1150-Co-60	Rutile, $CoTiO_3$	9850	55	44
*P*25	86% anatase, 14% rutile	29.5	48	0

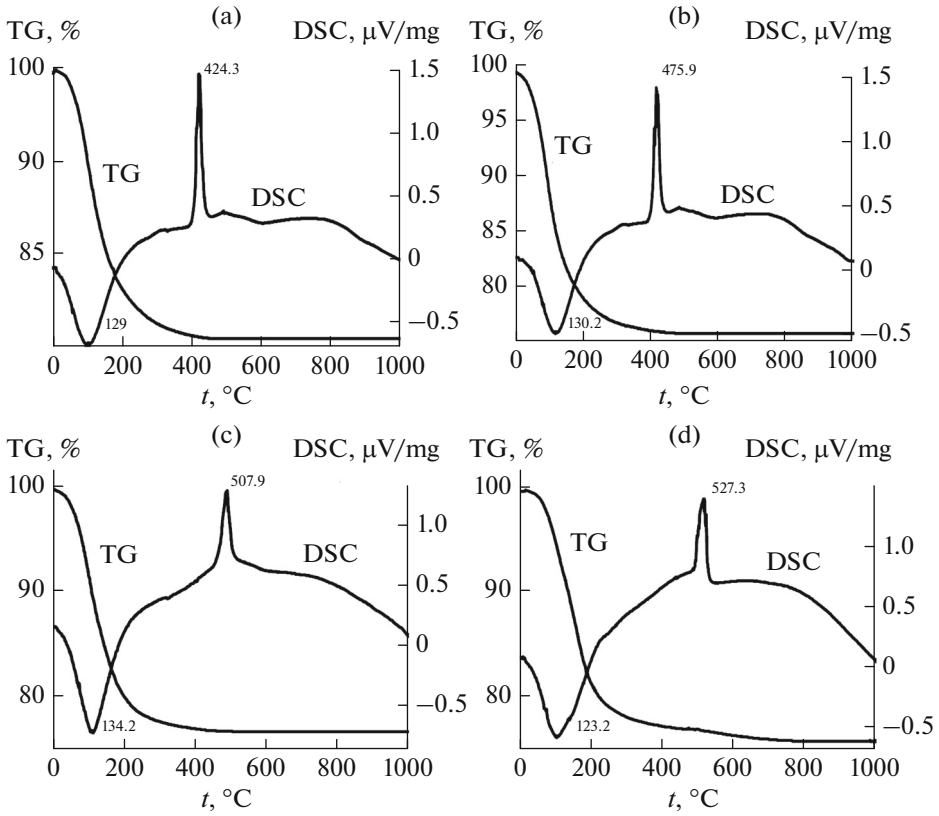

Fig. 3. Thermograms of the Co-modified titanium dioxide with respect to the Co content: (a) 0.5, (b) 5, (c) 10, (d) 40 wt %.

The depth and diameter of the pores in the samples that were heat-treated at up to 400°C have comparable sizes of 4.47 and 4.30 nm, respectively, for example, as in 400-Co-20. As the temperature exceeds 600°C, the pore diameter grows faster than the pore depth, i.e., 7.9 and 20.4 nm, respectively, in 800-Co-20, which indicates that the surface is getting smoother.

Thus, the both X-ray amorphous and crystalline polyphase composites with surface areas of approximately 15–330 m^2/g have a mesoporous structure in the Ti–O–Co system. The mesoporous materials are considered to be promising catalysts for the transformation of volumetric organic molecules, since the occurrence of mesosized pores can overcome diffusion restrictions [11] that are typical of microsized pores.

Morphology

The SEM-graphic image of the synthesized Co-containing products (Fig. 6) that were formed at temperatures of 400–1150°C shows their polydispersity, which manifests in the occurrence of both fine and large particles. Micrographic images demonstrate quite similar morphological changes that depend on heat treatment. The X-ray amorphous products are represented by extended layered irregular-shaped aggregates that are clusters of nanosized particles. As the temperature rises, the particles of all the samples first coalesce to form separate round-shaped crystallites. At 1150°C, they are calcined to massive hummocky formations with sizes up to a few dozen

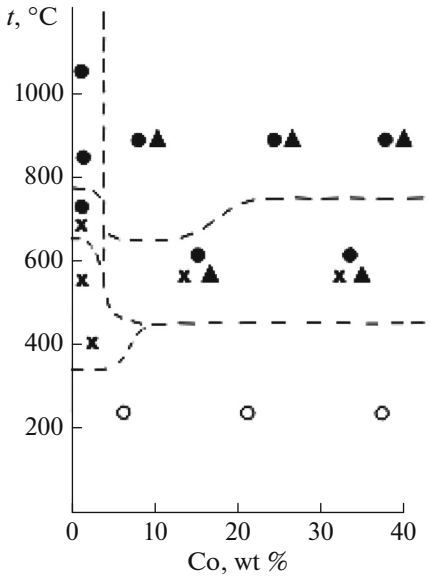

Fig. 4. Phase composition of synthesized composites with respect to the Co-content and temperature of heat treatment. Phases: ○ is X-ray amorphous, × is anatase, ● is rutile, ▲ is $CoTiO_3$.

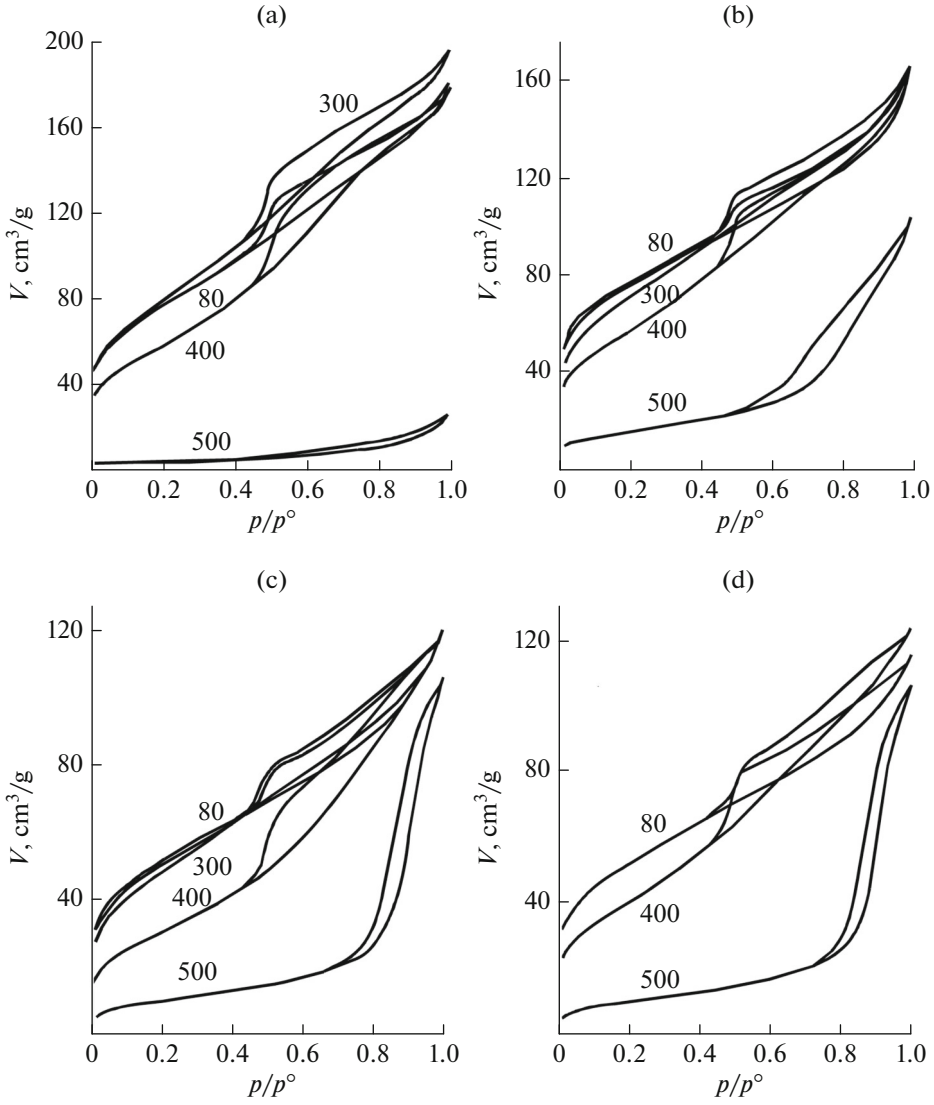

Fig. 5. Sorption isotherms of the synthesized composites after heat treatment at the different temperatures (numbers at the curves, °C) with respect to the Co content: (a) 5, (b) 20, (c) 30, (d) 40 wt %.

microns with smooth surfaces, which indicates the collapse of mesopores due to intense growth in unidentified crystals of rutile with cobalt titanate and their agglomeration.

Thus, the disproportions in the Ti–O–Co system causes the formation of the $TiO_2/TiO_2 \cdot CoTiO_3$ heterostructure or the $CoTiO_3/TiO_2 \cdot CoTiO_3$ heterostructure with objects located near each other that have different energies for the transition of an electron into a free state, which results in the enhancement of the photocatalytic properties of the synthesized composites.

Photocatalytic Activity

Preliminary studies of the PCA of the Co-modified titanium dioxide samples in the reaction of ferroin degradation, when the suspensions were exposed to visible light, its significant and complex dependence on the doping degree, the heat treatment, and consequently the phase composition were established. It has been shown that almost all Co-modified samples of TiO_2 have higher PCA relative to the Degussa AEROXIDE *P*25 photocatalyst (Table 3, Fig. 7) when they are exposed to the full spectrum of solar light and especially to the filtered light with $\lambda \geq 670$ nm, which conventionally corresponds to a decrease in the width of the energy of the composite forbidden band down to 1.85 eV. In this case, the maximum values of the PCA are demonstrated by the mesoporous X-ray amorphous and polyphase compositions with the most developed surface, and the minimum values are detected in the two-phase compositions that contain only rutile and cobalt metatitanate and are character-

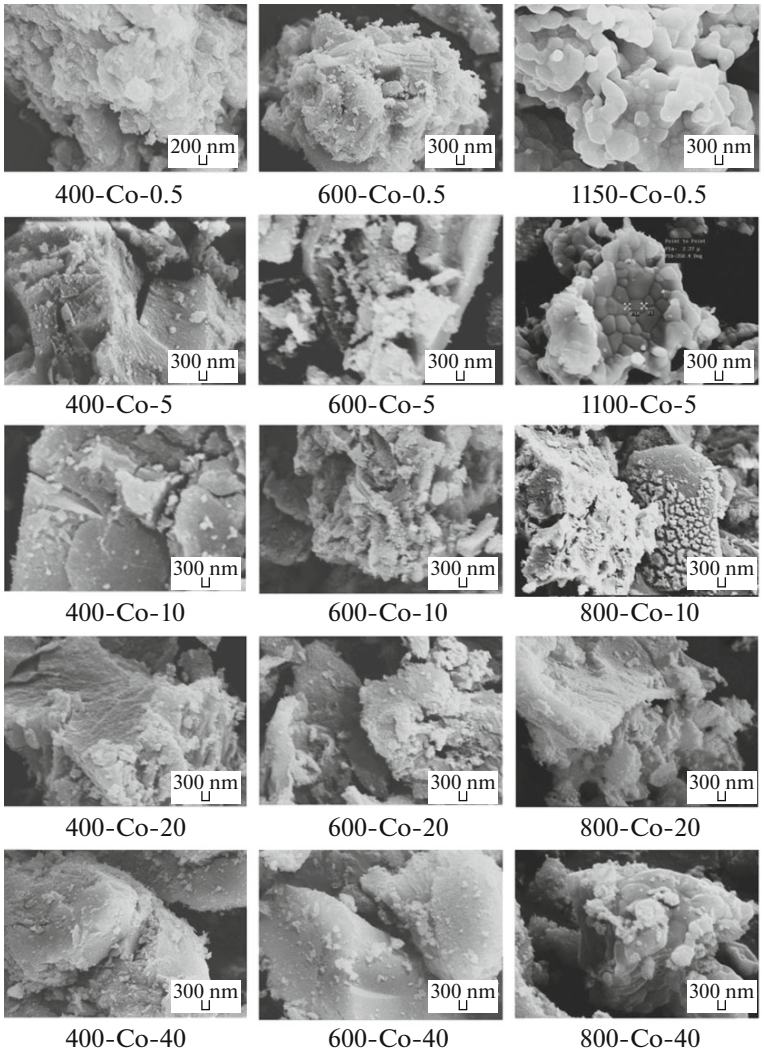

Fig. 6. SEM-graphic image for the surface of synthesized composite particles at 400–1150°C (phase composition is given in Fig. 4).

ized by the smallest surface area and the absence of mesoporosity. It is evident that the spectral sensibilization to the long-wave light region of nanocomposites is determined by Co together with the phase states of TiO_2 especially when the degree of Co doping is 10–20 wt %.

We note that, in our work, we confined ourselves to the light filter that detains the visible waves, whereas the forbidden bandwidth = 0.7 eV of the cobalt oxide also indicates the spectral sensibilization of the composites in the near-infrared region of light.

An analysis of the results of studying the adsorption (Fig. 8) as an important stage of photocatalysis points to the maximum values of adsorption A (mg/g) by X-ray amorphous powders that have the biggest surface area (heat treatment at 80–300°C). In addition to the more developed surface, the increased adsorption of the X-ray amorphous products may be related to the quite high concentration of polar hydroxyl groups of oxohydroxides that were not fully dehydrated. We also recorded the higher adsorption of ferroin by the low-doped samples Co-0.5–10 relative to TiO_2. The shrinkage of the surface area and the completion of the dehydration are likely to explain its decrease in the second temperature range of 300–700°C. Here, the composites show the fast coarsening of particles, which is nevertheless compensated for by the increasing depth and, especially, the pore diameter (Table 2).

The adsorption capacity of highly doped Co-20–40 samples decreases, as the Co content in the composite increases. However, for samples Co-40–60, the adsorption does not significantly depend on either the temperature or doping in the temperature range of 80–600°C. The PCA of these composites is also moderate compared to the others. One should note the stable adsorption characteristics of the composites in the temperature range of 400–800°C, where they exceed the adsorption properties of the pure TiO_2 regardless

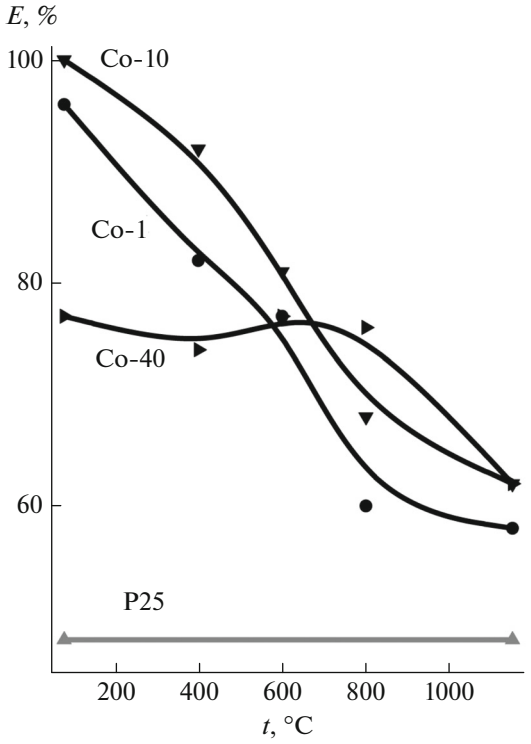

Fig. 7. Temperature dependence of FCA (E, %) for Co-modified titanium dioxide powders on Co doping (numbers on curves, wt %).

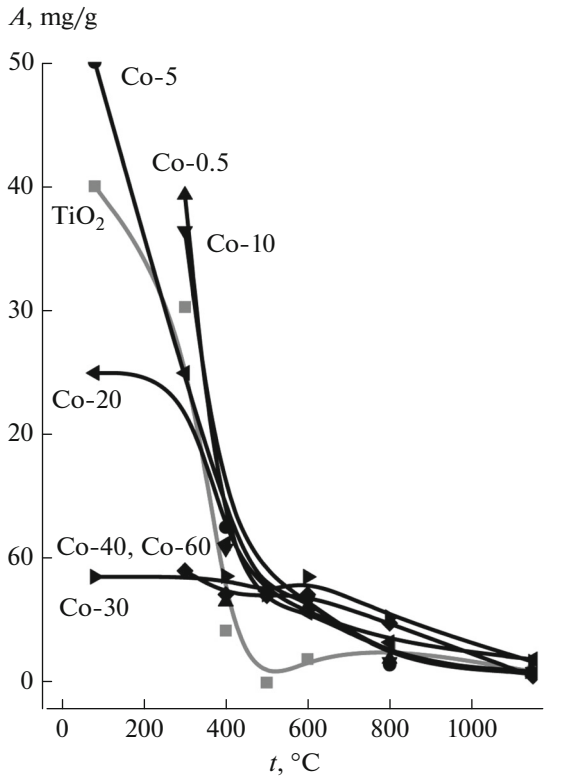

Fig. 8. Dependence of ferroin adsorption (A, mg/g) on Co-modified titanium dioxide on degree of doping and calcination temperature (t, °C).

of the degree of doping. A comparison of these data and the phase composition (Fig. 4) evidently shows that this region has already generated and successively intensifies the occurrence of crystalline phases, including anatase, rutile, and cobalt metatitanate. The increase in the adsorption of the powders of this genesis is likely to increase the PCA of the developed materials. In fact, the character of the smoother decrease in the temperature dependence of the PCA degree (Fig. 7) compared to the similar adsorption dependence that goes down more sharply (Fig. 8) indicates that the photocatalytic degradation of the indicator of certain physicochemical properties of the composites undergo an evident additional influence, which should be studied further.

The concentration dependence of the PCA (Fig. 9) of the composites that were obtained at temperatures up to 600°C has an extreme character. It is evident that Co doping in the range of 10–20 wt % contributes to the increase in the PCA degree relative to the more or less doped samples. The quite high values of the PCA of the samples that were calcined at temperatures of approximately 600°C, which provide the thermolysis of organic compounds indicate the possible regeneration of photocatalysts without losing their photocatalytic properties.

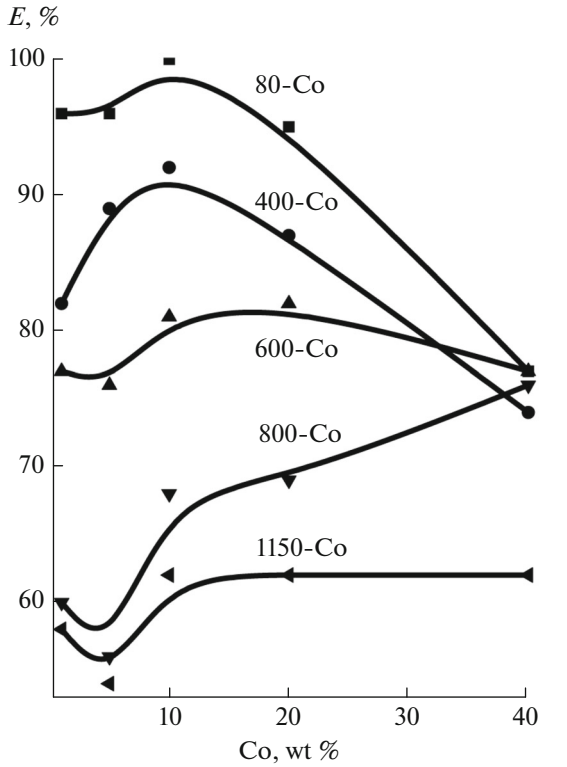

Fig. 9. Isotherms of FCA dependence (E, %) for synthesized composites with respect to Co content (temperatures, °C are numbers in sample marks on curves).

The experimental data confirm the idea about the expansion of the spectral range of TiO_2 FCA to the visible spectral range by creating the polyphase nanostructured composites that are formed by two semiconductors with different values of the forbidden bandwidth.

Studies of more detailed correlations of the physicochemical properties of the synthesized composites and their photoactivity in the visible and near regions of the infrared solar light will be continued.

CONCLUSIONS

The phase formation, texture, and photocatalytic activity of oxide nanocomposites of titanium(IV) and cobalt(II) were studied in relation to the cobalt content and heat treatment temperature. The high photocatalytic activity was recorded in optimum compositions exposed to visible light.

The increase in the PCA and spectral sensibilization at the light exposure with $\lambda \geq 670$ nm of relatively pure titanium dioxide are achieved due to the formation of the polyphase structures and the intensification of PC semiconducting properties when cobalt is added. In this case, mesoporous PC powders can be both X-ray amorphous and polyphase mixtures of X-ray amorphous products, anatase, rutile, and cobalt metatitanite with particles sized up to 100 nm.

The results can be used to develop highly effective catalysts.

ACKNOWLEDGMENTS

This work was supported by the program of the Institute of Semiconductor Physics, Russian Academy of Sciences, nos. 8 and 24, and the grant NSh 487,2014.3.

REFERENCES

1. Fenezonov, V.B. and Parmon, V.N., Introduction to the physical chemistry of the formation of the texture of heterogeneous photocatalysts, in *Promyshlennyi kataliz v lektsiyakh* (Lectures on Industrial Catalysis), Moscow: Kalvis, 2005.
2. Jin, Q., Fujishima, M., and Tada, H., Visible-light-active iron oxide-modified anatase titanium(IV) dioxide, *J. Phys. Chem. C,* 2011, vol. 115, no. 14, pp. 6478–6483.
3. Sedneva, T.A., Lokshin, E.P., Belikov, M.L., and Kalinnikov, V.T., Photocatalytic activity of tungsten-modified titanium dioxide, *Dokl. Phys. Chem.,* 2012, vol. 443, no. 1, pp. 57–59.
4. Sedneva, T.A., Lokshin, E.P., Belikov, M.L., and Belyaevskii, A.T., TiO_2- and Nb_2O_5-based photocatalytic composites, *Inorg. Mater.,* 2013, vol. 49, no. 4, pp. 382–389.
5. Samsonov, G.V., Bulankova, T.G., and Burykina, A.L., *Fiziko-khimicheskie svoistva okislov. Spravochnik* (Physical and Chemical Properties of Oxides. A Handbook), Moscow: Metallurgiya, 1969.
6. Zhang Guoge, Huang Haitao, Li Wenfang, Yu Fei, Wu Huijun, and Zhou Limin, Enhanced photocatalytic activity of CoO/TiO_2 nanotube composite, *Electrochim. Acta*, 2012, vol. 81, pp. 117–122.
7. Xu Rui, Li Jia, Wang Jun, Wang Xiaofang, Liu Bin, Wang Baoxin, Luan Xiaoyu, and Zhang Xiangdong, Photocatalytic degradation of Er^{3+} organic dyes under solar light irradiation combined with Er^{3+}: $YAlO_3$/Fe- and Co-doped TiO_2 coated composites, *Sol. Energy Mater. Sol. Cells*, 2010, vol. 94, no. 6, pp. 1157–1165.
8. Carvalho, H.W.P., Batista, A.P.L., Bertholdo, R., Santilli, C.V., Pulcinelli, S.H., and Ramalho, T.C., Photocatalyst TiO_2–Co: The effect of doping depth profile on methylene blue degradation, *J. Mater. Sci.*, 2010, vol. 45, no. 20, pp. 5698–5703.
9. Surkin, R.R., Zhimalov, A.B., Bondareva, L.N., Gorina, I.N., Gerancheva, O.E., and Polkan, G.A., RF Patent 2434819, 2011.
10. Ivanova, V.P., Kasatov, B.K., Krasavina, T.N., and Rozinova, E.L., *Termicheskii analiz mineralov i gornykh porod* (Thermal Analysis of Minerals and Rocks), Leningrad: Nedra, 1974.
11. Gregg, S.J. and Sing, K.S.W., *Adsorption, Surface Area and Porosity*, London: Academic, 1982.

Translated by L. Mukhortova